Available online at www.eccomasproceedia.org
Eccomas Proceedia COMPDYN (2017) 4509-4526

ECCOMAS
Proceedia

COMPDYN 2017
6th ECCOMAS Thematic Conference on
Computational Methods in Structural Dynamics and Earthquake Engineering
M. Papadrakakis, M. Fragiadakis (eds.)
Rhodes Island, Greece, 15–17 June 2017

EFFECT OF MAJOR SEISMOLOGICAL PARAMETERS ON DIRECTIVITY DOMINANT SPECTRAL AMPLIFICATION (COMPDYN 2017)

Saed Moghimi[1], **Sinan Akkar**[2]

[1] Department of Civil Engineering, Middle East Technical University
06800 Ankara, Turkey
e-mail: Saaed_m@yahoo.com

[2] Department of Earthquake Engineering, Bogazici University
34684 Istanbul, Turkey
sinan.akkar@boun.edu.tr

Keywords: Directivity, Narrow-band model, Pulse period, Pulse type ground motion, Response spectrum

Abstract. *One of the most important features of directivity-dominant near-fault ground motions is the existence of impulsive signals in the beginning of ground velocity. Directivity is observed when rupture propagates toward a site at a velocity close to particle shear-wave velocity. Such ground motions with large-amplitude and long-period velocity pulses amplify the response spectrum in medium to long period ranges. As such, they have the potential to impose severe inelastic demands on the medium to high-rise buildings.*

In this study we discuss the differences between the directivity models proposed in NGA-WEST2 [i.e., Shahi and Baker and Chiou and Spudich presented in Spudich et al. (2013)] and Shahi and Baker (2011). Deterministic and probabilistic seismic hazard analyses are done with and without considering directivity effects for different earthquake scenarios as well as 475-year and 2475-year return periods. The response spectrum amplification due to directivity is extracted from these hazard analyses and the effects of major seismological parameters on the computed spectral amplifications are investigated. The observed results suggest some differences in the investigated directivity models for deterministic and probabilistic earthquake scenarios. The characteristic magnitude and fault-site geometry play an important role in all models within probabilistic hazard framework. The Shahi and Baker directivity models also bring forward the significance of slip rate and return period in spectral amplifications. The slip rate and return period do not prominently affect the spectral amplifications in Chiou and Spudich directivity model. The observations suggest a need for the consideration of forward directivity on code-based design spectrum via some practical rules.

© 2017 The Authors. Published by Eccomas Proceedia.
Peer-review under responsibility of the organizing committee of COMPDYN 2017.
doi: 10.7712/120117.5741.18397

1 INTRODUCTION

One of the important features of near fault ground motions is directivity effect. In near fault earthquakes when rupture propagates toward a site a pulse is formed in the beginning of the velocity wave form. These pulses are mostly seen in the fault normal direction. This kind of records which have higher amplitude with shorter duration are known as ground motions with forward directivity effect. On the other hand when rupture propagates away from the site the ground motion will have lower amplitude with longer duration. This case is called backward directivity.

Housner and Trifunac (1967) were the first that observed ground motions with long period, strong velocity and displacement pulses in 1966 Parkfield earthquake. The second earthquake with impulsive signal in fault normal component was reported in 1971 San Fernando earthquake (Boore & Zoback 1974; Niazy 1975). Bertero et al. (1978) have studied destructive effect of pulse type ground motions on medium to high-rise buildings for the first time. However, 1994 Northridge earthquake was the first that revealed vulnerability of high-rise buildings against pulse type ground motions. Later on the observations from 1995 Kobe, 1999 Izmit and 2009 L'Aquila Earthquakes confirmed the previously seen destructive potential of the near-fault impulsive ground motions (Alavi & Krawinkler 2001; Chioccarelli & Iervolino 2010).

Some of design codes incorporated the effects of near fault ground motions after the destructive potential of these ground motions were identified. Uniform Building Code (UBC, 1997) applies a uniform scaling on the design spectrum with 475-year return period for the near fault effects of ground motions. Near source effects are defined with Na (for short period range of design spectrum) and Nv (for long period range of design spectrum) factors in UBC, 1997. These factors are applied on the seismic coefficients Ca and Cv for the sites located in high seismicity regions (seismic zone 4).

In order to better estimate the effects of near fault impulsive ground motions the directivity effect is needed to be incorporated in ground motion models. Traditional ground-motion models do not account for the effect of pulse-like ground motions and hence, they may under predict the spectral acceleration for impulsive ground motions in medium to high period ranges depending on earthquake magnitude. Several researchers have proposed different directivity models to be implemented on ground motion equations.

One of the first important directivity models was proposed by Somerville et al. (1997). This model basically uses two geometric parameters to assemble the directivity effect on ground motion equations. First, the angle between the direction of rupture propagation and the direction of waves traveling from the fault to the site, second, the fraction of the fault rupture surface that lies between the hypocenter and the site. Somerville et al. (1997) modifies ground motion average horizontal response spectral acceleration, and duration of acceleration time history in order to incorporate directivity effect in ground motion equations. The model also proposes a ratio for strike normal to strike parallel component of ground motions with directivity effect. This model was modified by Abrahamson (2000) in order to incorporate the magnitude and distance saturation in directivity model.

Shahi and Baker (2011) (hereafter SHB-11) used together with Boore and Atkinson (2008) (hereafter BA-08) have calibrated a new framework on the PSHA in order to incorporate directivity effect. The method first has been proposed with Tothong et al. (2007) which considers the probability of pulse occurrence and pulse period in hazard analysis. Iervolino and Cornell (2008) have used the source to site geometrical parameters used in this model in order to quantify the probability of pulse occurrence.

Although some primary models have been proposed for directivity in NGAWEST1 (2008) project but they did not include directivity and guidance for its application in their equations explicitly. The most recent and comprehensive directivity models have been proposed by NGA-WEST2 Directivity Working Group (Spudich et al. 2013). This report include five directivity models. The models proposed by Roshandel, Shahi & Baker (hereafter SHB-13), Spudich & Chiou (models proposed in chapter 3, 4 and 5 in Spudich et al. 2013) are explicitly narrow-band in which the spectral acceleration is amplified in a narrow range of periods close to pulse period. Bayless & Somerville (the model proposed in chapter 2 in Spudich et al. 2013) have updated Somerville et al. (1997) directivity model which is a broad-band model and amplifies the response spectrum uniformly in medium to high spectral period ranges. Chiou & Spudich (hereafter CHS-13) (the model proposed in chapter 6 in Spudich et al. 2013) uses Directivity Predictor Parameter (DPP) as the predictor of directivity together with ground motion equation proposed by Chiou and Young (2014) (hereafter CHY-14).

In this study we have discussed the theoretical and mathematical differences between SHB-11, SHB-13 and CHS-13 directivity models. The results will be discussed in terms of deterministic and probabilistic hazard analysis. In deterministic analysis the variation of amplification factor for three cases has been studied and discussed. The comparisons and discussions are done on the basis of deterministic hazard analysis. In addition Probabilistic Seismic Hazard Analysis has been done in order to investigate the effect of earthquake scenarios and source to site geometric parameters on the level of amplification due to directivity. In PSHA SHB-11and CHS-13 directivity models have been assembled in a Matlab code that has been written for this purpose. Uniform hazard spectrum has been extracted for each site with and without considering directivity effect for two return periods (475 and 2475-Year). SH-11 and CHS-13 models have been used for calculation of response spectrum with directivity effect. Response spectrum without directivity effect is calculated with conventional probabilistic seismic hazard analysis. The amplification is calculated from the normalization of spectral acceleration with directivity effect to spectral acceleration of conventional PSHA.

In the next section general framework of SHB-11, SHB-13 and CHS-13 directivity models have been described. The geometric illustrations and the differences among these models will be illustrated and explained. Selection of input parameters for the seismic hazard analysis and the effect of these parameters on the level of amplification will be discussed in the next sections of this study.

2 INTRODUCTION OF DIRECTIVITY MODELS

2.1 General Framework of Shahi and Baker 2011 (SHB-11)

The general framework of this method is to some extend different from the conventional PSHA methods. This model considers the probability of pulse occurrence and pulse period distribution in hazard analysis. Equation (1) shows the annual exceedance rate of spectral acceleration with directivity effect:

$$\nu_{Sa}(x) = \sum_{i=1}^{\#\,faults} \nu_i \iiint P^*\left(S_a > x \mid m,r,z,t_p\right).f_i(m,r,z).dm.dr.dz.dt_p \qquad (1)$$

where m, r, z and t_p represent magnitude, distance, source to site geometry and pulse period parameters respectively. The PSHA model proposed in Equation 1 can be practically evaluated by splitting $P^*\left(S_a > x \mid m,r,z,t_p\right)$ into two cases, depending on whether or not pulse-like ground motion is observed. These two cases are shown in Equation 2.

$$P^*(S_a > x \mid m,r,z) = P(pulse \mid m,r,z).P(S_a > x \mid m,r,z,pulse) + [1 - P(pulse \mid m,r,z)].P(S_a > x \mid m,r,no\ pulse) \quad (2)$$

Regarding this model the spectral acceleration is amplified for pulse like ground motions and de-amplified for non-pulse like cases. In this method the probability of pulse occurrence depends on source to site geometric parameters.

2.2 Chiou and Spudich-2013 (CHS-13) Directivity Model

Chiou and Young (2014) have adapted a directivity model (f_{DPP}) on their Ground Motion Equation (CHY-14) in order to incorporate effect of near fault impulsive ground motions in response spectrum estimation. This model uses Direct Point Parameter (DPP) as the predictor of directivity effect. The functional form of f_{DPP} is shown in Equation 3 in which f_R and f_M are distance and magnitude taper functions represented in Equations 4 and 5 respectively.

$$f_{DPP} = c_8 . f_R . f_M . e^{-c_{8a}(M - c_{8b})^2} . \Delta DPP \quad (3)$$

$$f_R = \max[0, 1 - \frac{\max(R_{rup} - 40)}{30}] \quad (4)$$

$$f_M = \max[1, \frac{\max(M - 5.5, 0))}{0.8}] \quad (5)$$

In Equation 3, c_8 and c_{8b} are period dependent coefficients and c_{8a} is period independent coefficient given in Chiou and Young (2014). The distance taper function reduces f_{DPP} effect to zero starting from 40 to 70km. The magnitude taper also has the same function for the magnitude range 6.3 to 5.5. This is due to the fact that directivity effect is not seen in larger distances and smaller magnitude ranges. ΔDPP in Equation 3 is centered value of direct point parameter. Since conventional ground motion equations take some account of rupture directivity effects in the average sense due to existence of pulse type ground motions in the dataset used to develop these equations the directivity models cannot be used directly as an add-on directivity correction in these equations. Therefore a centering value of directivity parameter is used in directivity model. The centered value of DPP has been defined in CHS-13 model and it is calculated from Equation 6 for a specific site in which $\overline{DPP}$ is the average value of DPP for the sites with a constant distance from the fault rupture.

$$\Delta DPP_i = DPP_i - \overline{DPP} \quad (6)$$

DPP has three factors, a measure of isochrone velocity ($\hat{c}'$); a measure of rupture propagation distance (E); and a radiation pattern term ($\overline{FS}$). DPP is calculated from Equation 7 for a single planar rupture surface.

$$DPP = ln(\hat{c}'.max(E, 0.1f) . max(\overline{FS}, 0.2)) \quad (7)$$

In this equation E is the distance between hypocenter (P_H) and direct point (P_D), f is the larger of fault length and width, $\overline{FS}$ is the average S-wave radiation pattern over E-Path and $\hat{c}'$ is the isochrone velocity which is calculated from Equation 8.

$$\hat{c}' = \frac{1}{(\frac{1}{0.8} - \frac{R_{HYP} - R_D}{E})} \quad \text{for E>0}$$
$$\hat{c}' = 0.8 \quad \text{for E=0} \quad (8)$$

where R_{HYP} is hypocenter to site distance (P_HP_S) and R_D is the direct point to site distance (P_DP_S).

2.3 Chiou and Spudich-2013 (CHS-13) Directivity Model

This model extends the approach of SHB-11 in order to incorporate directivity effect in Ground Motion Equations. The model is composed of two parts as can be seen in Equation 9. The first term is the base Ground Motion Equation which predicts the natural logarithm of spectral acceleration in spectral period of T seconds.

$$lnSa_{ij} = f(M_i, R_j, T, Vs30_j, \theta, \dots) + I_{directivity}.\ln amp\,(T, T_p) + \eta_i + \varepsilon_{ij} \qquad (9)$$

The first term is a function of magnitude, distance, period and shear wave velocity of the site. The coefficients in the base ground motion model (θ) are refitted without considering directivity effect. In this way the directivity effect which is implicitly included in the original Ground Motion Equation due to existence of pulse type ground motions in the dataset is removed. The second term amplifies the base ground motion model due to existence of impulsive period which is the function of spectral period and pulse period ratio as can be seen in Equation 10. $I_{Directivity}$ is a binary value which takes one when the ground motion contains a pulse and takes zero otherwise.

$$\ln amp\,(T, T_p) = b_0.\exp\left(b_1(\ln\left(\frac{T}{T_p}\right) - b_2)^2\right) \qquad (10)$$

the coefficients have been determined from refitting the ground motion model to the NGA-WEST2 data set. Finally η_i and ε_{ij} in Equation 9 are between-event and within-event errors respectively.

2.4 COMPARISION OF SHB-11, SHB-13 AND CHS-13 DIRECTIVITY MODELS

As stated before SHB-13 is extended version of SHB-11 and therefore the general framework and utilized geometric parameters in the both models are similar to each other. Both models are narrow-band which amplify the ground motion spectral acceleration at periods close to pulse period. These two models also have differences in terms of mathematical form and development procedure. SHB-11 de-amplifies the spectral acceleration for non-pulse cases while SHB-13 uses the spectral acceleration of base ground motion equation without applying any de-amplification for these cases. Both of the models use the same source to site geometric models which are illustrated in Figure 1.

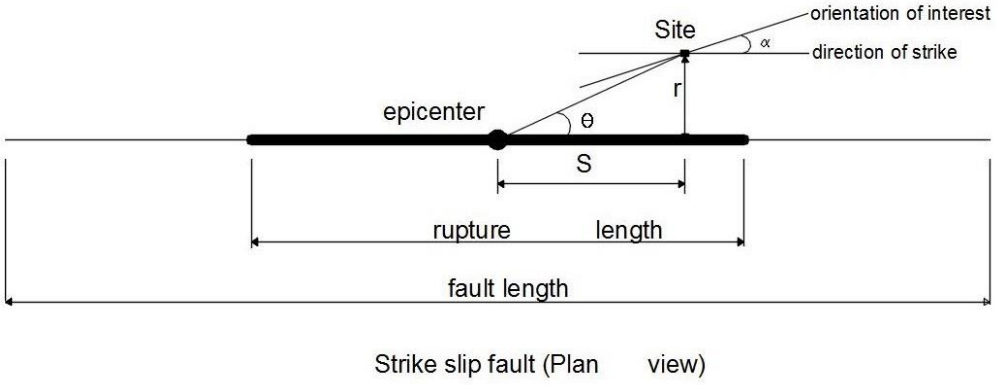

Figure 1 Source to site geometric parameters of SHB-11 and SHB-13 models for Strike Slip Faults

In this figure "r" is the closest distance of the site to the rupture and "s" is the rupture length that lays between the hypocenter and closest distance of the site to the fault in the fault strike direction and θ is the angle between fault strike direction and the line that joins epicenter and the site. These parameters (r, s and θ) are used to calculate probability of pulse occurrence distribution pattern around the fault in SHB-11 and SHB-13 directivity models.

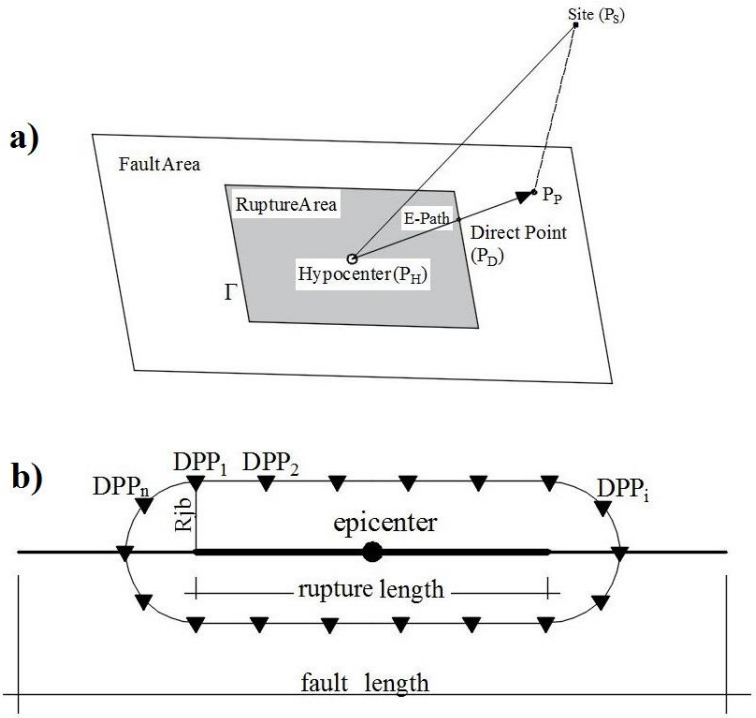

Figure 2 CHS-13 model a) Source to site geometric parameters b) Direct Point Parameter distribution around the rupture

As stated in section 2.2 CHS-13 model uses Direct Point Parameter (DPP) as the predictor of directivity effect. In this model the direct point concept (DP) is the intersecting point of the fault-projected direct ray ($P_H P_P$) with the slipped-area boundary, where P_H is the hypocenter and P_P is the projection of the site onto the plane containing the slipped area (Figure 2a). When a site is normal to the slipped area (i.e., P_P is inside slipped area), the direct point is the same as Pp (P_D and P_P will coincide on each other). Direct point concept (DP) in CHS-13 is used to define centered value of Direct Point Parameter (ΔDPP) as shown in Figure 2b.

The other difference between these models is the component that they predict for ground motion spectral acceleration. SHB-11 model is used together with Boore and Atkinson (2008) (BA-08) Ground Motion Equation in order to investigate the directivity effect. BA-08 predicts RotI50 component of ground motion and SHB-11 modifies RotI50 component to predict spectral acceleration in a desired orientation with respect to fault strike direction for pulse type ground motions. SHB-13 uses Refitted Campbell and Bozorgnia (2008) (CBR) Ground Motion Equation in order to predict the spectral acceleration with directivity effect. Therefore this model modifies RotD50 component of the ground motion model in a desired orientation in order to predict spectral acceleration with directivity effect. On the other hand, CHS-13 directivity model is adapted on Chiou and Youngs (2014) (CHY-14) Ground Motion Equation which estimates RotD50 component. Therefore CHS-13 modifies RotD50 component to estimate RotD50 component with directivity effect ($RotD50_{Directivity}$).

3 SELECTION OF INPUT PARAMETERS FOR HAZARD ANALYSIS

This study aims to investigate the effect of seismological and geometrical parameters on the level of amplification for considered directivity models. For this purpose we have run both Deterministic and Probabilistic Seismic Hazard Analysis for different earthquake scenarios with these directivity models. Gridded mesh of 42 sites spatially distributed around the fault have been selected for the analysis in order to investigate the effect of source to site geometry on the amplification of response spectrum. The distances in fault strike direction (X direction) are normalized to the fault length and this normalized distance is measured from the center of the fault projection on the ground. The fault length is taken as "L" and the sites are extended 0.3×L beyond the fault edge in X direction. In addition, the sites are placed every 5km in the fault normal direction (Y direction) from 0 to 30km. Due to symmetry sites are scattered just in upper right quarter of the fault (Figure 3).

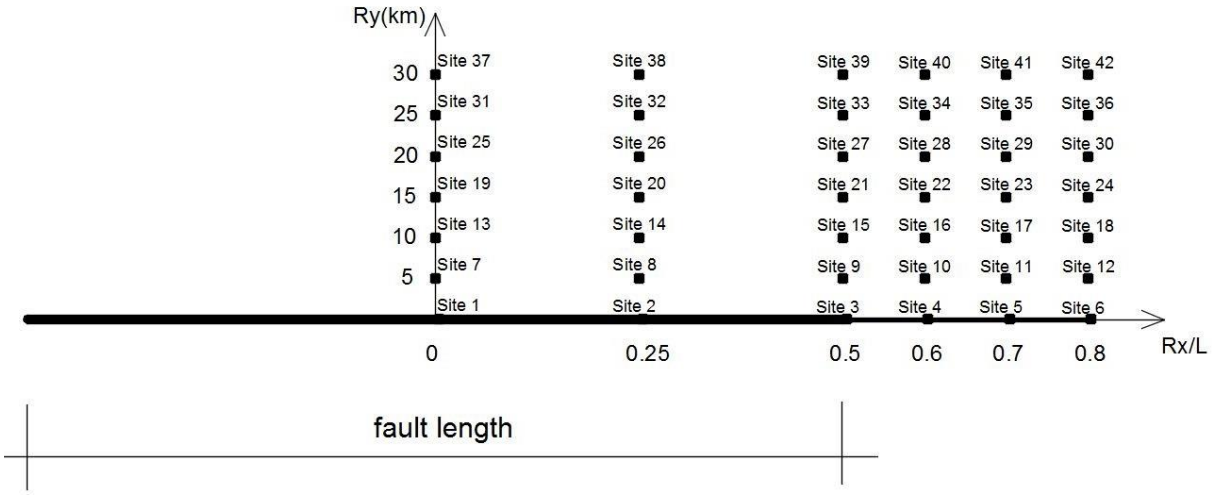

Figure 3 Gridded sites around the fault for investigation of Source to site geometry effect

The other parameter that can play important role on the amplification of response spectrum due to directivity effect is the earthquake magnitude. Five different faults with different characteristic magnitudes have been selected for the hazard analysis in order to investigate the effect of this parameter on the amplification. As mentioned before pulse-type ground motions with directivity effect are mostly seen in earthquakes with medium to large magnitude. Therefore the faults are selected in a way that their characteristic magnitude represent this magnitude range. The faults are selected with 20, 50, 100, 150 and 300km length and 10km width for all cases with characteristic magnitudes equal to 6.25, 6.7, 7.0, 7.2 and 7.5 respectively. Characteristic earthquake reccurence model (Youngs & Coppersmith 1985) has been used in all the hazard analysis. The earthquake magnitudes greater than 5 have been considered in probabilistic hazard analysis.

The other important parameter than can be effective on the level of amplification is the slip rate of the fault. Three slip rate values have been assigned to the faults (SR=0.5, 1.0 and 2.0 cm/year) for the analysis indicating low, medium and high seismicity levels.

4 DISCUSSIONS ON DETERMINISTIC HAZARD ANALYSIS

In deterministic hazard analysis the spectral acceleration is calculated for a single earthquake scenario. In our case we have calculated the amplification of spectral acceleration with

three directivity models discussed in the last sections. The amplification has been calculated for a fault with 100km length, slip rate 1.0 cm/year and for the sites 8, 9 and 10 (illustrated in Figure 3) which are located 5km away from the fault in Y direction. Figure 4 illustrates the median of spectral acceleration calculated for site 9 with and without considering directivity effect for SHB-11, SHB-13 and CHS-13 directivity models. As can be seen from this figure the SHB-11 has the largest amplification in a narrow period range. But the point that should be considered here is that SHB-11 combines amplification and de-amplification cases in a full probabilistic analysis. The de-amplification case is shown with **SHB 11-NoDirectivity** dotted line in this figure. In order to better see the difference between these models we have plotted the spectral amplification of three directivity models for sites 8, 9 and 10 in Figure 5.

In SHB-11 and SHB-13 the amplification is the same for all three sites (8, 9 and 10) since the amplification is just a function of T/Tp parameter which is the same for all of these three sites. In SHB-11 the Deamplification is the same for site 8 and 9 because the deamplification term is a function of magnitude and distance. For the site 8 and 9 the magnitude and distance parameters are equal (M_{ch}= and Rjb=5km). In Site 10 we do not observe any deamplification because there is a distance cap for the deamplification factor which makes it equal to 1 for the distances greater that 10km (note that Rjb of site 10 is 11.18km). The overall amplification in SHB-11 is calculated from the combination of pulse and no pulse cases for the full probabilistic seismic hazard analysis.

In CHS-13 we observe an increasing trend for the Amplification while we are moving from site 8 toward site 10. This is due to the fact that the directivity effect is a function of ΔDPP (Chiou and Youngs 2014). Since ΔDPP has an increasing trend while moving from site 8 toward site 10 the amplification also shows the same trend.

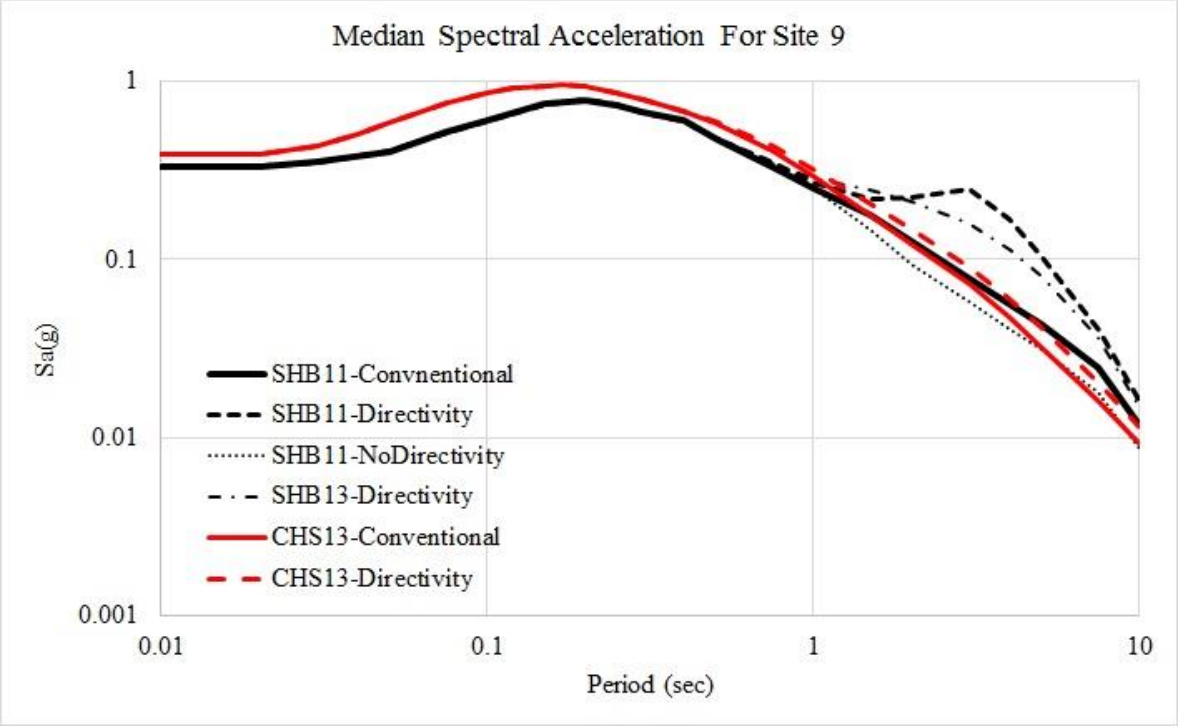

Figure 4 Median of spectral acceleration for Site 9 and earthquake scenario with FL=100 and SR=1cm/year calculated by DSHA

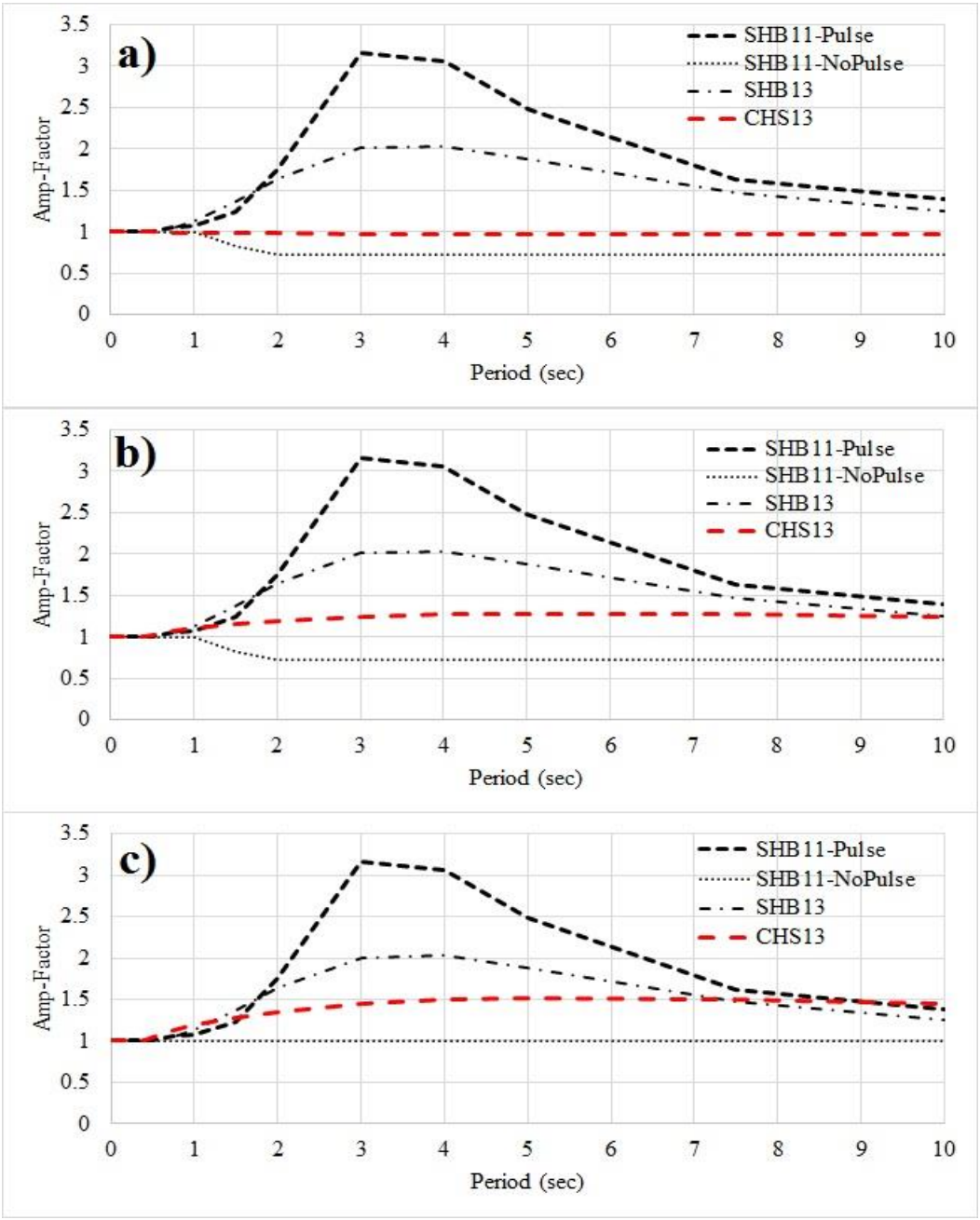

Figure 5 Amplification factor calculated with three directivity models
a) FL=100km, SR=1.0cm/year, Site 8 b) FL=100km, SR=1.0cm/year, Site 9
c) FL=100km, SR=1.0cm/year, Site 10

5 AMPLIFICATION INVESTIGATION FOR PSHA

In this section we have investigated the effect of source to site geometry, slip rate, fault magnitude and the hazard level (return period of response spectrum) on the level of amplification when PSHA is applied on the directivity models. All the considered faults are planar with the strike slip mechanism. The amplification factor is the ratio of uniform hazard spectrum calculated with SHB-11, and CHS-13 directivity models to conventional response spectrum (Equation 11).

$$AMP(T) = \frac{Sa(T)_{directivity}}{Sa(T)_{conventional}} \tag{11}$$

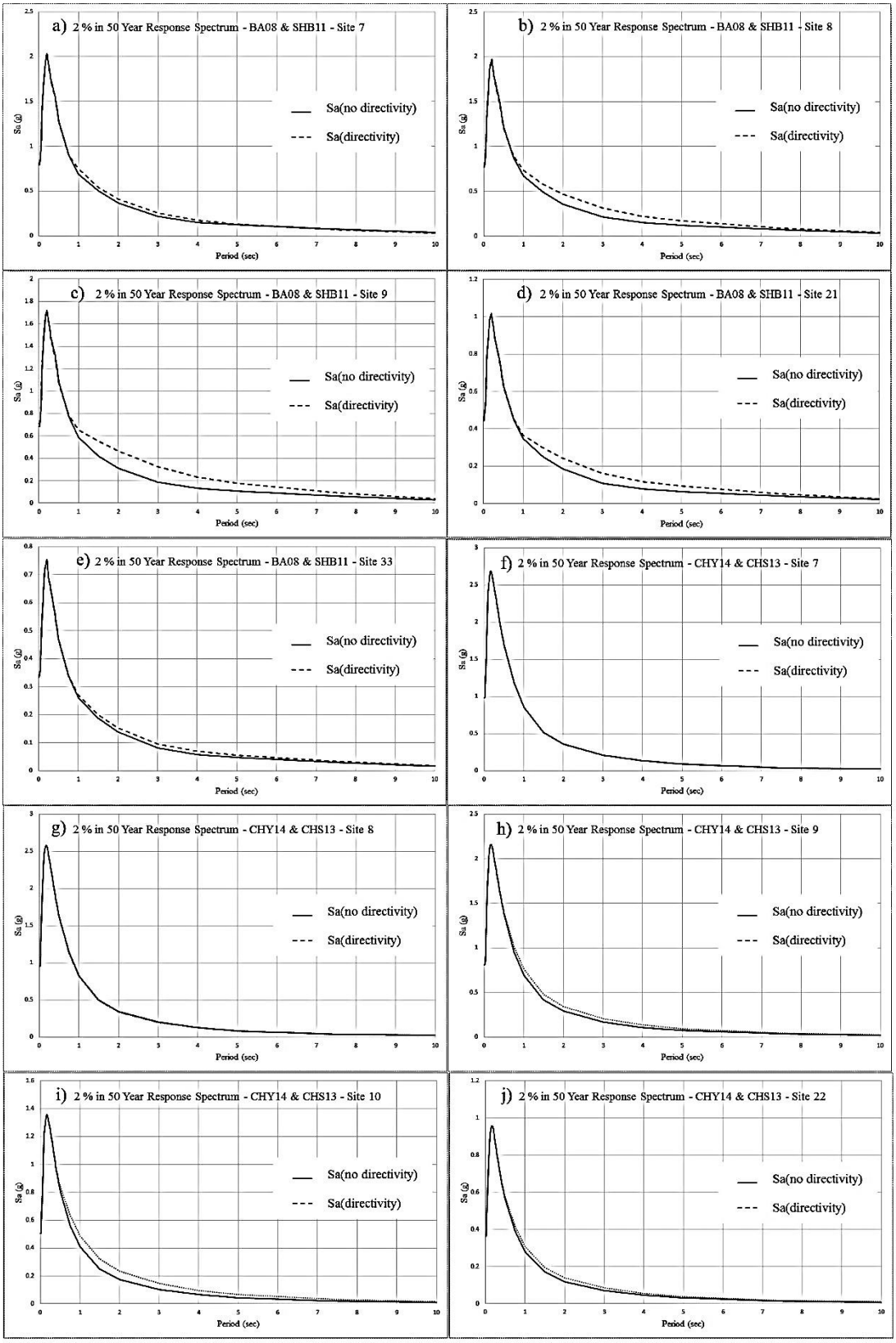

Figure 6 Effect of site location on the amplification due to directivity for SHB-11 and CH-13 models

5.1 Source to site geometry effect on the amplification factor

In order to better understand how source to site geometry affect on the level of amplification the hazard analysis have been done for different sites scattered spatially around the fault. Response spectrum has been extracted for each site with and without considering directivity effect. The distribution pattern of the sites around the fault has been shown in Figure 3.

In Figure 6a, to 6e we have compared the response spectrum from conventional PSHA with response spectrum calculated from SHB-11 model for different source to site locations around the fault. The site which is located on the Rx/L=0 and Ry=5km (Site 7 shown in Figure 6a) is amplified very slightly and the amplification is almost close to 1. The amplification increases when we move from site 7 (Rx/L=0 and Ry=5km) toward the edge of the fault in X direction. The maximum amplification is reached for the site located on Rx/L=0.5 and Ry=5km (Site 9 in Figure 6c). On the other hand when we move away from the fault in Y-direction (from Site 9 toward Site 33 shown in Figure 6c, 6d and 6e) the amplification has a descending trend. This amplification pattern for different source to site geometries is due to the source to site geometric parameters used to calculate probability of pulse occurrence in SHB-11.

In Figure 6f to 6j the response spectrum calculated with CHS-13 model is compared with conventional response spectrum for different source to site locations. In this model also we don't observe any amplification for site 7 (Figure 6f) like SHB-11 model. Unlike SHB-11 model the ascending trend of amplification in X direction for CHS-13 model starts from site 8 (Rx/L=0.25 and Ry=5km) and reaches its maximum in Site 10 (Rx/L=0.6 and Ry=5km). This is due to the effect of centered value of DPP (Direct Point Parameter) in this model. As stated before E-path parameter is used to calculate the DPP for each site. This parameter (E-path which is distance between hypocenter and direct point) reaches its maximum values for the sites located along the Rx/L=0.6 line. Therefore the ΔDPP and subsequently the amplification will be maximum for these sites.

In Y direction the amplification of CHS-13 model also has descending trend like SHB-11 model. This can be seen if we compare the amplification level of site 10 (shown in Figure 6i with Rx=0.6 and Ry=5km) with site 22 (shown in Figure 6j with Rx/L=0.5 and Ry=15km). In site 22 the response spectrum extracted with CHS-13 model is slightly larger than conventional response spectrum meaning that amplification level is slightly larger than 1.

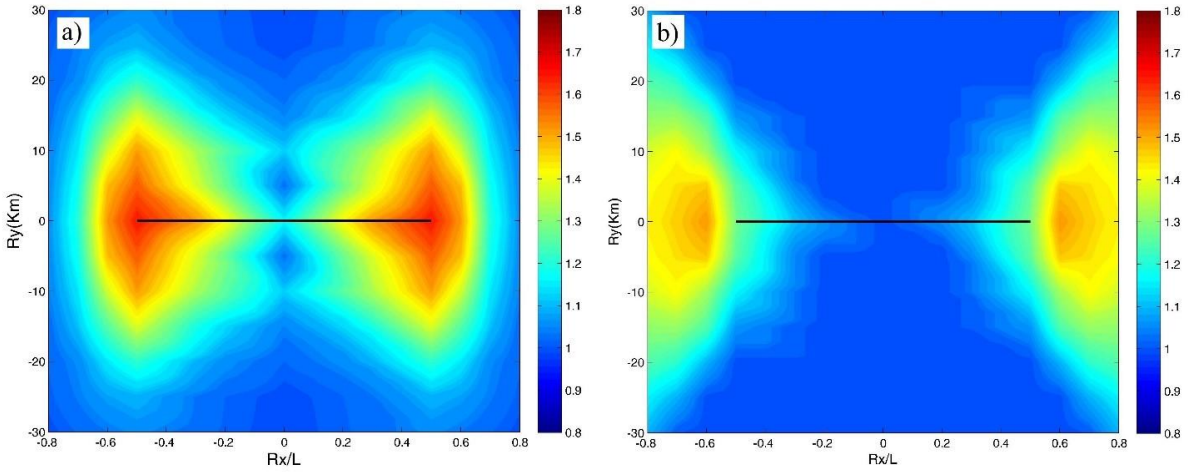

Figure 7 Amplification factor contour map for 100km length fault, Slip rate=2cm/year and 475 year return period spectrum, T=4sec. a) Shahi and Baker 2011, b) Chiou Spudich 2013

In order to better see the amplification distribution pattern around the fault, the contour maps of amplification have been plotted for a fault with 100km length, slip rate 2cm/year and 475 year return period at spectral period T=4sec. The Figure 7a shows the amplification contour map for SHB-11 model and Figure 7b is the counter map of amplification for CHS-13 model. The location of the sites which experience maximum amplification, the variation of the amplification pattern along X and Y directions and the differences between these two models which were discussed in previous paragraphs can be seen in this figure very clearly.

5.2 Effect of Hazard Level and Slip Rate on the Amplification Factor

As stated before three slip rate values (SR=0.5, 1, 2 cm/year) have been considered in the probabilistic hazard analysis for low medium and high seismicity levels. The amplification factor has been calculated for all the sites around the fault (42 sites) and two hazard levels (2% and 10% probability of exceedance in 50 year). These amplification factors have been plotted for all 42 sites together with their median values for SHB-11 model in Figure 8. As can be seen from this figure all the amplification curves reach their maximum value at spectral period T=4 sec for the fault with 100km length. The general shape of the amplification curves are similar to each other in all figures with just one exception in Figure 8a.

In this figure (Figure 8a) we see a bump for the amplification curves in small period ranges. This is due to the fact that SHB-11 model does not apply deamplification for the magnitudes less than 6, Rjb larger than 10km and spectral periods smaller than 1sec for non-pulse type cases. On the other hand large magnitude earthquakes do not contribute effectively in hazard analysis for this case. Therefore the larger period ranges are not amplified as much as small magnitude ranges for 475 year return period case.

The results of the analysis from SHB-11 model (Figure 8) show that both slip rate and return period are determining parameters on the level of amplification factor. For both 2% and 10% in 50 year exceedance hazard levels the amplification factor increases with slip rate increment. This increment can be seen in both median and maximum amplification factor curves. The important point here is that the rate of increment for the sites which are more exposed to directivity effect (the sites that experience larger amplification values) is more than the other sites when slip rate increases from 0.5 to 2 cm/year. This can be seen more clearly if we compare the maximum values of amplification for 10% in 50 year exceedance cases. Table 1 shows the maximum and median amplification values at T=4sec for two hazard levels. The maximum amplification of the fault with SR=0.5 cm/year at spectral period T=4sec is 1.19 (Figure 8a) while this maximum value for the case of SR=1.0 cm/year reaches 1.38 (Figure 8c) and for the SR=2.0cm/year it reaches to 1.65 (Figure 8e). This is equivalent to 16% and 38% increase for the maximum amplification of SR=1.0 and 2.0 cm/year from maximum amplification of SR=0.5 cm/year. For the median values at the same spectral period the amplification increases from 1.04 for SR=0.5 cm/year to 1.10 and 1.16 for SR= 1.0 and 2.0 cm/year respectively which is equivalent to 5.7% and 11.5% increment. As can be seen the rate of amplification increment for the maximum and the median values are not the same.

The difference between the maximum and median amplification indicates the importance of source to site geometry because the median amplification is the mean of lnAMP of all 42 sites amplification factor. On the other hand the rate of amplification increment is different for maximum and median amplification. This means that slip rate and source to site geometry are correlated to each other and the amplification level cannot be estimated for each of these parameters independently.

We can also see the same trend for the case of 2475 year return period (2% in 50 year exceedance) amplification factor. First, the maximum and median amplification factors are not the same for a given slip rate value. Second, the amplification increases with the slip rate in-

crement for both median and maximum amplification curves but the rate of this increment for maximum and median values are not the same.

The last thing that can be seen in this model is that the amplification of 2475 year return period (2% in 50 year exceedance) has larger values comparing to the amplifications of 475 year return period (10% in 50 year exceedance). The maximum amplification shows a 43% increment for the case of SR=0.5cm/year and 13.3% for the fault with SR=2.0cm/year when return period changes from 475 to 2475 year.

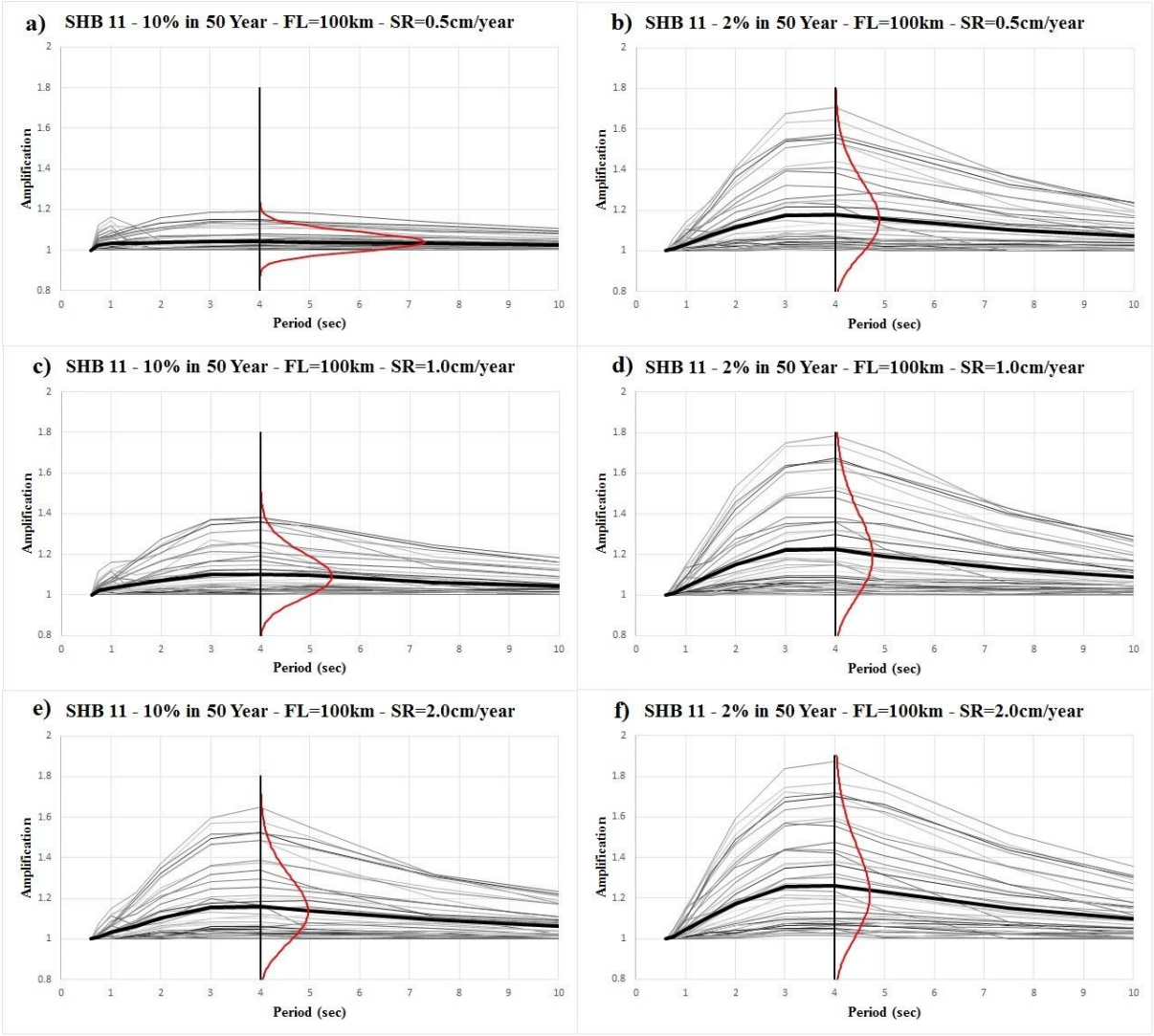

Figure 8 Effect of slip rate and return period on the amplification in SHB-11 model

	10% in 50 year exceedance (475 year RP)		2% in 50 year exceedance (2475 year RP)	
	AMP_{max}(T=4sec)	AMP_{median}(T=4sec)	AMP_{max}(T=4sec)	AMP_{median}(T=4sec)
SR=0.5	1.19	1.04	1.71	1.18
SR=1.0	1.38	1.10	1.79	1.22
SR=2.0	1.65	1.16	1.87	1.26

Table 1 Maximum and median amplification at T=4sec for the faults with SR=0.5, 1 and 2cm/year-SHB-11 model

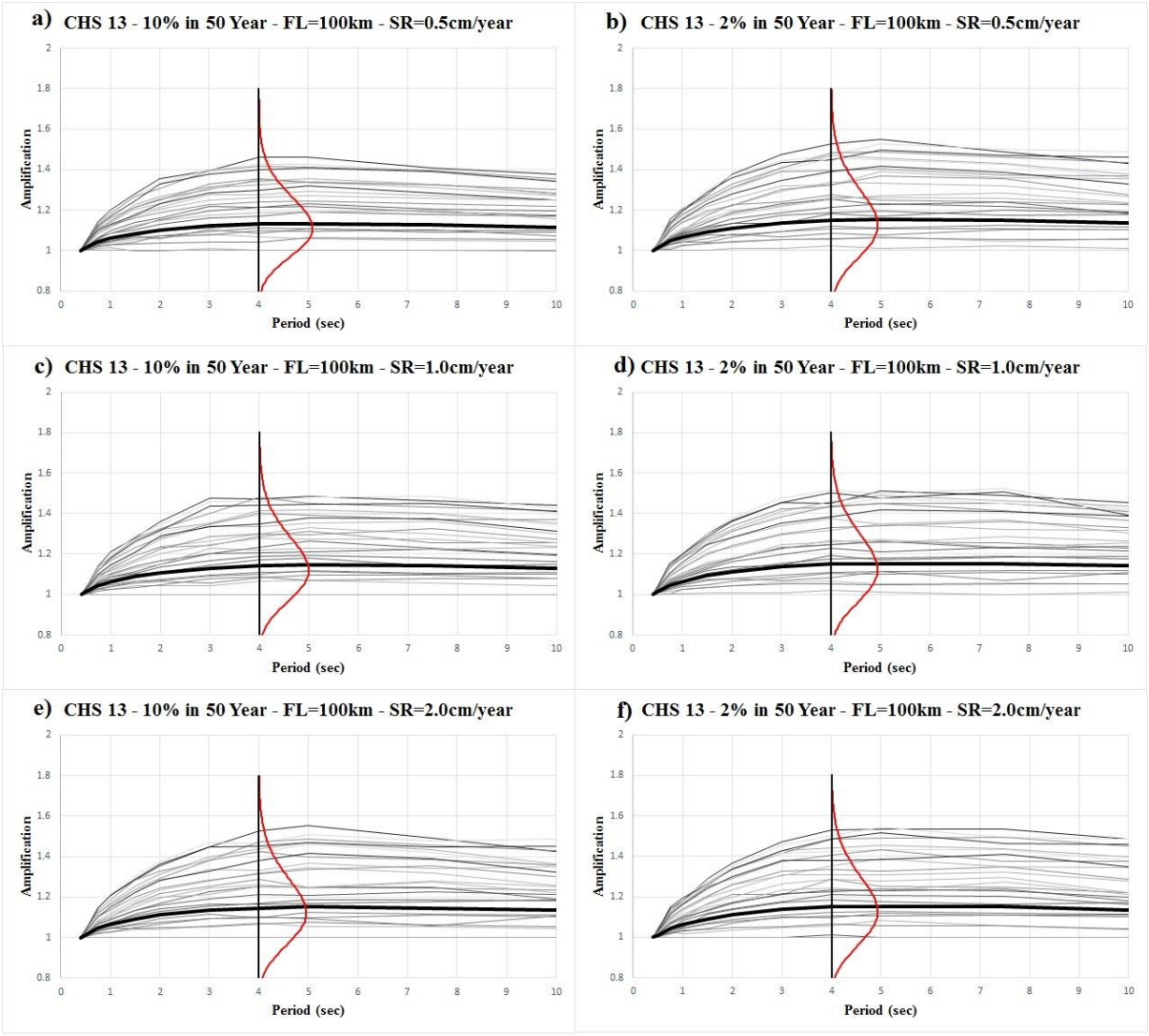

Figure 9 Effect of slip rate and return period on the amplification in CHS-13 model

	10% in 50 year exceedance (475 year RP)		2% in 50 year exceedance (2475 year RP)	
	AMP_{max}(T=4sec)	AMP_{median}(T=4sec)	AMP_{max}(T=4sec)	AMP_{median}(T=4sec)
SR=0.5	1.45	1.13	1.52	1.15
SR=1.0	1.47	1.14	1.5	1.15
SR=2.0	1.52	1.15	1.53	1.15

Table 2 Maximum and median amplification level at T=4 sec for the faults with SR=0.5, 1 and 2cm/year-CHS-13 model

Figure 9 shows the amplification curves of CHS-13 model for a fault with 100km length, slip rate=0.5, 1.0 and 2cm/year and 2 hazard levels (10% and 2% exceedance rate). The maximum and median of amplification factor for 42 sites are shown in Table 2 for 3 slip rate values and 2 hazard levels at spectral period T=4sec.

The results of the analysis for this model also shows several observations. First, the amplification level is not affected by slip rate values. As can be seen from Figure 9 and the results given in Table 2, the maximum amplification do not change considerably when slip rate increases from 0.5cm/year to 2.0cm/year for both 475 and 2475 year return period cases. Fur-

thermore the median amplification value is almost the same for all slip rate values and hazard levels.

The other important point is the difference between maximum and median amplification for a given slip rate and hazard level. As stated before since all source to site geometries contribute on the amount of median amplification it shows that that source to site geometry is still determining parameter on the level of amplification.

The last point here is the effect of return period on the level of amplification. As can be seen from Table 2 the maximum and median amplification factor do not change considerably for these two hazard levels. The amplification of 2475 year is slightly larger than amplification of 475 year but this difference is less than 4% in the worst case. Therefore it can be concluded that CHS-13 model is not affected by slip rate and hazard level considerably but source to site geometry still has important effect on the level of amplification.

5.3 Effect of Fault Characteristic Magnitude on the Amplification Factor

The last parameter that has been investigated in this study is the effect of fault characteristic magnitude on the level of amplification. Figure 10 shows the amplification factor for two faults with different characteristic magnitudes for both SHB-11 and CHS-13 models. Several features can be seen in this figure. Both SHB-11 and CHS-13 models have a bilinear trend for the amplification factor. The difference between these two models is that SHB-11 model tends to amplify the response spectrum in a narrow range of period while CHS-13 model amplifies the spectrum in a wider range of periods. This is due to the fact that SHB-11 model tries to amplify the Sa at periods close to the period of the directivity pulse (Tp). The amplification factor in SHB-11 reaches the maximum value at a spectral period (T_{max}) followed by a descending trend for larger periods. The amplification factor in CHS-13 has an ascending trend up to spectral period called as T_{corner}. For the periods greater than T_{corner} the amplification has plateau form and is almost constant.

In SHB-11 model the amplification amplitude starts from 1.0 at spectral period T=0.6sec and reaches the maximum amplitude at T_{max}=3.0sec for the fault with 50km length and characteristic magnitude equal to 6.7. For the fault with 150km length and characteristic magnitude 7.2 the amplification amplitude starts from 1.0 at spectral period T=0.6sec and reaches the maximum amplitude at spectral period T_{max}=4 sec. In CHS-13 the amplification amplitude starts from 1.0 at spectral period T=0.5sec and reaches the maximum amplitude at T_{corner}=3.0sec for the fault with 50km length and T_{corner}=4.0sec for the fault with 150km length. As can be seen, the spectral period that maximum amplification occur in both SHB-11 and CHS-13 models depend on characteristic magnitude of the fault, meaning that the larger is the characteristic magnitude, the greater is the spectral period that maximum amplification occur.

Fault magnitude can also affect on the amplitude of amplification. As can be seen from Figure 10 the amplitude of amplification increases with fault magnitude for both SHB-11 and CHS-13 models. Faults with greater magnitude have greater amplification amplitude especially in the period range that the maximum amplification occur.

The results of analysis have also shown that increment of amplification amplitude due to characteristic magnitude increase, show a saturation for the faults with characteristic magnitude greater than 7.5. The results confirms that the maximum amplification for the fault with characteristic magnitude 7.75 is slightly larger than the maximum amplification of the fault with characteristic magnitude 7.5 for both SHB-11 and CHS-13 models. This is due to the effect of distance taper functions used in the directivity models, because the sites located in one

edge of fault which experience the maximum amplifications, are too far from the ruptures that occur on the other edge of the fault.

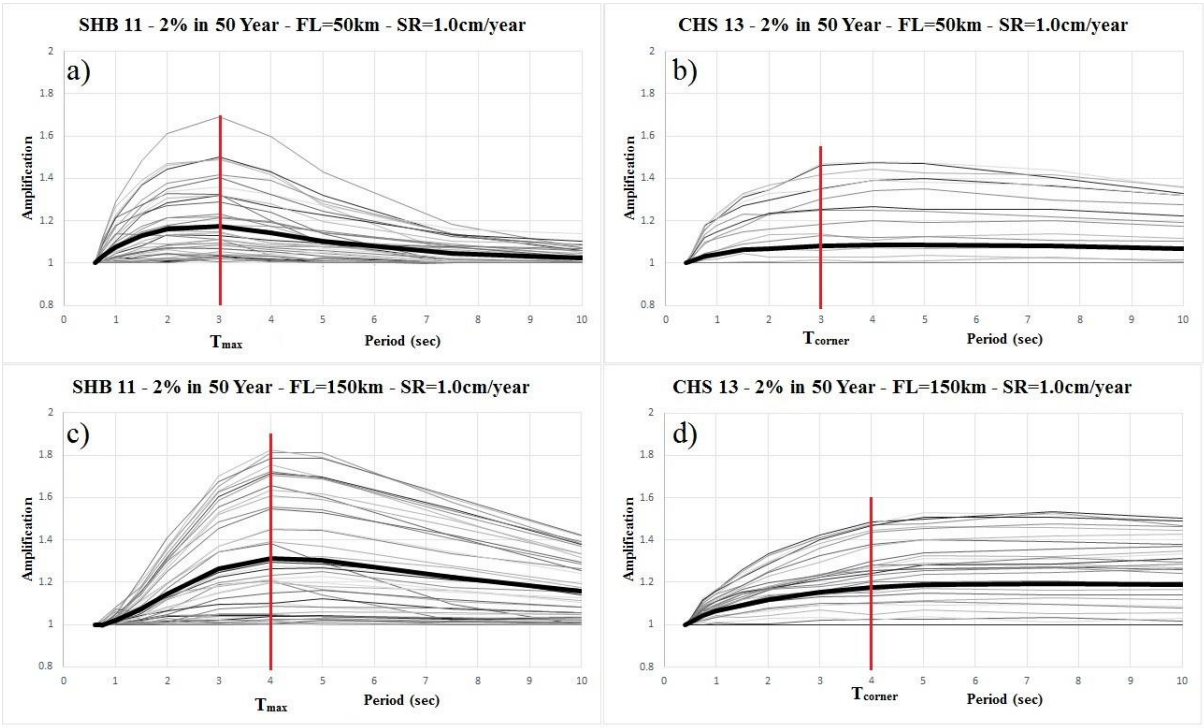

Figure 10 Effect of characteristic magnitude of the fault on the amplification factor in SHB-11 and CHS-13 models

6 CONCLUSIONS

- The results of Deterministic Hazard Analysis have shown that the general trend of amplification pattern is the same for SHB-11 and SHB-13 directivity models. Both of these models amplify the response spectrum proportional with T/Tp ratio. The probability of pulse occurrence also contribute on the level of amplification in these models in terms of source to site geometric parameters.
- In CHS-13 the amplification is a function of DPP which is directivity indicator parameter in this model.
- According to PSHA results the maximum amplification occur on the sites located near the fault edges in SHB-11 model while the maximum amplification occur on the sites located beyond the fault edges in CHS-13.
- PSHA results shows that the amplification factor in SHB-11 model is a coupled function of slip rate, fault magnitude, source to site geometry and hazard level all together. But it has been shown that amplification factor in CHS-13 model is not affected by slip rate and hazard level and it is a function of fault characteristic magnitude and source to site geometry.

REFERENCES

[1] Abrahamson, N. A. (2000). Effects of rupture directivity on probabilistic seismic hazard analysis. In *Proceedings of the Sixth International Conference on Seismic Zonation: Managing Earthquake Risk in the 21st Century, Palm Springs, CA, 12-15 November 2000*. Retrieved from http://nisee.berkeley.edu/elibrary/Text/200803124

[2] Alavi, B., & Krawinkler, H. (2001). *Effects of Near Fault Ground Motions on Frame Structures*. *Blume Earthquake Engineering Center, Report No. 138, Department of Civil and Environmental Engineering, Stanford University, CA*. Retrieved from http://blume.stanford.edu/

[3] Bertero, V., Mahn, S., & Herrera, R. (1978). Aseismic design implications of near-fault San Fernando earthquake records. *Earthquake Engineering & Structural Dynamics*, *6*(July 1976), 31–42. http://doi.org/10.1002/eqe.4290060105

[4] Boore, D. M. (2010). Orientation-Independent, Nongeometric-Mean Measures of Seismic Intensity from Two Horizontal Components of Motion. *Bulletin of the Seismological Society of America*, *100*(4), 1830–1835. http://doi.org/10.1785/0120090400

[5] Boore, D. M., & Atkinson, G. M. (2008). Ground-motion prediction equations for the average horizontal component of PGA, PGV, and 5%-damped PSA at spectral periods between 0.01 s and 10.0 s. *Earthquake Spectra*, *24*(1), 99–138. http://doi.org/10.1193/1.2830434

[6] Boore, D. M., Watson-Lamprey, J., & Abrahamson, N. A. (2006). Orientation-Independent Measures of Ground Motion. *Bulletin of the Seismological Society of America*, *96*(4A), 1502–1511. http://doi.org/10.1785/0120050209

[7] Boore, D. M., & Zoback, M. D. (1974). Two-dimensional kinematic fault modeling of the Pacoima Dam strong-motion recordings of the February 9, 1971, San Fernando earthquake. *Bulletin of the Seismological Society of America*, *64*(3–1), 555–570. Retrieved from http://bssa.geoscienceworld.org/content/64/3-1/555%5Cnfiles/772/Boore_Zoback_1974_Two-dimensional kinematic fault modeling of the Pacoima Dam strong-motion.pdf%5Cnfiles/808/555.html

[8] Chioccarelli, E., & Iervolino, I. (2010). Near-source seismic demand and pulse-like records: A discussion for L'Aquila earthquake. *Earthquake Engineering and Structural Dynamics*, *39*(9), 1039–1062. http://doi.org/10.1002/eqe.987

[9] Chiou, B. S. J., & Youngs, R. R. (2014). Update of the Chiou and Youngs NGA model for the average horizontal component of peak ground motion and response spectra. *Earthquake Spectra*, *30*(3), 1117–1153. http://doi.org/10.1193/072813EQS219M

[10] Housner, G. W., & Trifunac, M. D. (1967). Analysis of accelerograms--Parkfield earthquake. *Bulletin of the Seismological Society of America*, *57*(6), 1193–1220. Retrieved from http://www.bssaonline.org/cgi/content/abstract/57/6/1193

[11] Iervolino, I., & Cornell, C. A. (2008). Probability of occurrence of velocity pulses in near-source ground motions. *Bulletin of the Seismological Society of America*, *98*(5), 2262–2277. http://doi.org/10.1785/0120080033

[12] Kramer, Steven L., (1996). Geotechnical Earthquake Engineering, Publ. Prentice Hall.

[13] McGuire, R. K. (2004). *Seismic Hazard and Risk Analysis*. *Book*. Earthquake Engineering Research Institute.

[14] Niazy, A. (1975). An exact solution for a finite, two-dimensional moving dislocation in an elastic half-space with application to the San Fernando earthquake of 1971. *Bulletin of the Seismological Society of America*, *65*(6), 1797–1826.

[15] Rowshandel, B. (2010). Directivity correction for the next generation attenuation (NGA) relations. *Earthquake Spectra*, *26*(2), 525–559. http://doi.org/10.1193/1.3381043

[16] Shahi, S. K. (2013). *A probabilistic framework to include the effects of near-fault directivity in seismic hazard assessment*. Stanford University, Stanford, CA.

[17] Shahi, S. K., & Baker, J. W. (2011). An empirically calibrated framework for including the effects of near-fault directivity in probabilistic seismic hazard analysis. *Bulletin of the Seismological Society of America*, *101*(2), 742–755. http://doi.org/10.1785/0120100090

[18] Somerville, P. G., Smith, N. F., Graves, R. W., & Abrahamson, N. A. (1997). Empirical strong ground motion attenuation relations to include the amplitude and duration effects of rupture directivity. *Seismological Research Letters*, *68*(1), 199–222. http://doi.org/10.1785/gssrl.68.1.199

[19] Spudich, P., Bayless, J. R., Baker, J., Chiou, B. S. J., Rowshandel, B., Shahi, S., & Somerville, P. (2013). *Final Report of the NGA-West2 Directivity Working Group*. *Pacific Engineering Research Center Report PEER Report 2013/09. NGA west 2 Database*.

[20] Spudich, P., & Chiou, B. S. J. (2008). Directivity in NGA earthquake ground motions: Analysis using isochrone theory. *Earthquake Spectra*, *24*(1), 279–298. http://doi.org/10.1193/1.2928225

[21] Tothong, P., Cornell, C. A., & Baker, J. W. (2007). Explicit directivity-pulse inclusion in probabilistic seismic hazard analysis. *Earthquake Spectra*, *23*(4), 867–891. http://doi.org/10.1193/1.2790487

[22] Wells, D. L., & Coppersmith, K. J. (1994). New Empirical Relationships among Magnitude, Rupture Length, Rupture Width, Rupture Area, and Surface Displacement. *Bulletin of the Seismological Society of America*, *84*(4), 974–1002. http://doi.org/

[23] Youngs, R. R., & Coppersmith, K. J. (1985). Implications of fault slip rates and earthquake recurrence models to probabilisic seismic hazrad estimates. *Bulletin of the Seismological Society of America*, *75*(4), 939–964.